Journal of the Society of Automotive Engineers Malaysia
Volume 9, Issue 2, pp 139-149, May 2025
e-ISSN 2550-2239

Comparative Finite Element Analysis of Triangulated Spaceframe Designs for Formula SAE Chassis under Static Load Conditions

M. H. A. Ali*[1,2], M. S. Mohamad[1,2], M. T. A. Rahman[2], M. N. Ayob[2], M. K. F. A. Rahman[2], M. F. M. A. Hamzas[2], A. Sanuddin[2], M. S. A. Fouzi[2], M. Y. R. Siahaan[3] and M. S. A. Kadir[4]

[1] Motorsport Technology Research Unit (MOTECH), Universiti Malaysia Perlis, 02600 Arau, Perlis, Malaysia
[2] Faculty of Mechanical Engineering Technology, Universiti Malaysia Perlis, 02600, Arau, Perlis, Malaysia
[3] Department of Mechanical Engineering, Faculty of Engineering, Universitas Medan Area, Indonesia
[4] Faculty of Mechanical Engineering, Universiti Teknologi Malaysia (UTM), 81310 Johor Bahru, Johor, Malaysia

*Corresponding author: husseinmuhd646@gmail.com

ORIGINAL ARTICLE **Open Access**

Article History:

Received
27 Mar 2025

Accepted
22 Apr 2025

Available online
1 May 2025

ABSTRACT – *This study presents a comprehensive finite element analysis of three Formula SAE spaceframe chassis configurations to evaluate their structural performance under standardized static load conditions. The analyzed chassis, designated as Design 1 (baseline), Design 2 (moderately reinforced), and Design 3 (fully triangulated), were subjected to five critical loading scenarios: front impact, main roll hoop, front roll hoop, lateral shear, and torsional deformation. The simulations were conducted using ANSYS Workbench with structural steel properties, and the results were benchmarked against a yield strength threshold of 305 MPa, corresponding to ASTM A36 mild steel. The analysis revealed that Design 3 demonstrated superior performance in terms of stiffness and safety due to its extensive triangulation and optimized load paths, particularly under torsional and frontal loads. Design 2, despite offering a lighter configuration, failed to satisfy yield criteria in multiple loading cases, highlighting the trade-off between weight reduction and structural integrity. These findings emphasize the critical role of triangulated architecture and nodal connectivity in achieving regulatory compliance and enhancing crashworthiness in Formula SAE chassis development.*

KEYWORDS: Formula SAE, spaceframe chassis, Finite Element Analysis (FEA), structural optimization, Von Mises stress

Journal homepage: www.jsaem.my

1. INTRODUCTION

The chassis of a Formula SAE (FSAE) race car serves as the primary load-bearing framework, linking the front and rear suspensions while providing mounting points for all essential components. It plays a critical role in ensuring occupant protection during impacts and in maintaining the vehicle's structural integrity under various static and dynamic load conditions (Patil & Chikkali, 2020). The FSAE technical regulations require structural compliance under specific load cases, including frontal collisions, lateral impacts, and rollover scenarios, to ensure driver safety and maintain minimal deformation (SAE, 2024; Khot et al., 2025). In addition, a well-designed chassis must exhibit high torsional rigidity, which is essential for accurate suspension response and vehicle handling (Riley & George, 2002; Wang et al., 2020).

To meet these demands while minimizing weight, finite element analysis (FEA) has become a standard tool in the early-stage design and validation of spaceframe structures (Patil & Chikkali, 2020; Patel et al., 2019). FEA enables engineers to simulate stress and deformation under worst-case loading conditions, identify critical stress points, and optimize member arrangements before fabrication (Patel et al., 2019). FSAE teams often use beam or shell elements in ANSYS or similar platforms to ensure the design satisfies the von Mises yield criterion, which is commonly used for ductile metals like steel (Thosar et al., 2016).

One fundamental principle in spaceframe design is triangulation, which enhances stiffness by ensuring that members primarily carry axial loads rather than bending moments (Ulizio et al., 2017). Proper triangulation improves load distribution, reduces stress concentrations, and allows designers to achieve higher stiffness with minimal material usage (Stava et al., 2012). Studies consistently demonstrate that a fully triangulated frame performs significantly better under torsional and impact loads than one with large, unbraced rectangular sections (Alirezaei et al., 2016).

The most used material for FSAE spaceframes is mild steel tubing, such as ASTM A36 or AISI 1020, due to its favorable combination of cost, weldability, and ductility (Lim & Sivaguru, 2018; Chen & Harichandran, 1998). In simulation, however, teams frequently substitute structural steel, which shares nearly identical elastic properties (E ≈ 200 GPa, σ_y ≈ 250 MPa), making it a valid proxy for FEA (Khutal et al., 2020). This substitution does not affect stiffness predictions and, if anything, results in conservative stress estimates due to slightly lower default yield values in software environments (Lim & Sivaguru, 2018).

This study evaluates three spaceframe chassis configurations with increasing complexity and triangulation. Each design is assessed using ANSYS Workbench under five standardized static load cases: front impact, main roll hoop, front hoop, lateral shear, and torsional loading. Von Mises stress and total deformation are computed and benchmarked against the 250 MPa yield strength of mild steel. This comparative FEA provides actionable insights into how structural optimization, specifically triangulation and node bracing, influences stress distribution, stiffness, and overall crashworthiness in Formula SAE chassis design.

2. METHODOLOGY

2.1 Chassis Design Configurations

Three tubular spaceframe chassis configurations – Design 1 (baseline), Design 2 (moderately reinforced), and Design 3 (fully triangulated) – were developed in compliance with FSAE regulations, sharing identical overall dimensions (roll hoop heights, driver cockpit, wheelbase) but differing in internal bracing and load path optimization. Design 1 (Figure 1) employs a minimalist layout with rectangular side bays (upper/lower rails and vertical hoops), basic front/rear roll-hoop supports, and no diagonal reinforcements, rendering sections such as the floor and side bays prone to bending and torsional deformation. Design 2 (Figure 2) introduces strategic improvements, including a diagonal brace in the side bays to form triangular trusses, a mid-wheelbase floor cross-member for torsional rigidity, and reinforced nodal connections at roll hoop junctions to distribute stress. Design 3 (Figure 3) represents the fully optimized configuration, featuring X-braced side bays and floor planes for maximum stiffness, rearward braces from the front hoop to the upper chassis, and a triangulated rear roll hoop structure. This design ensures loads are transmitted axially rather than through bending, with all rectangular openings replaced by triangulated segments. While Design 3 incorporates more tubing (and thus higher mass), it achieves superior structural efficiency, minimizing stress concentrations and deformation under load. To ensure the accuracy of the analysis results, when geometrically modelling the framework, a 1:1 three-dimensional model is established.

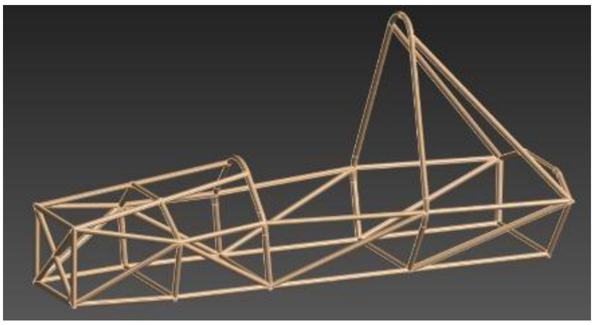

FIGURE 1: Baseline chassis configuration (Design 1)

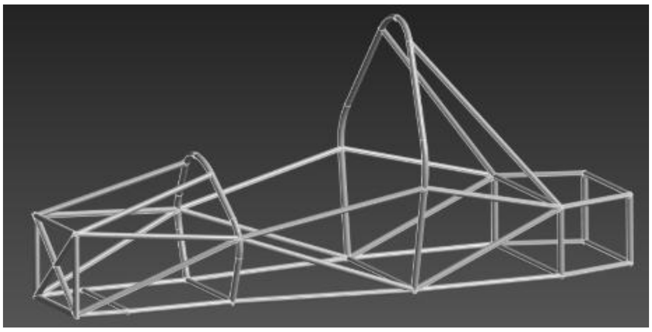

FIGURE 2: Moderately reinforced chassis configuration (Design 2)

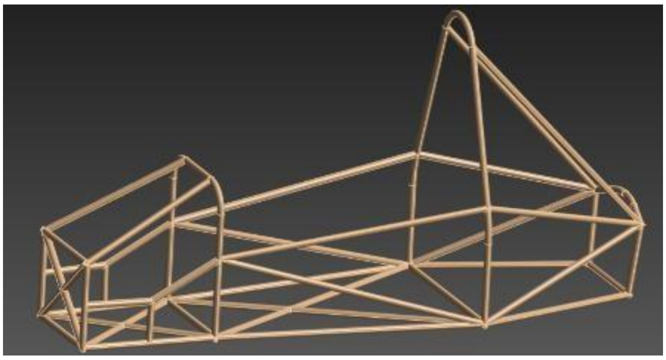

FIGURE 3: Fully triangulated chassis configuration (Design 3)

2.2 Finite Element Modelling

The three-dimensional CAD models of the chassis designs were imported into ANSYS Workbench at a 1:1 scale to ensure geometric fidelity. Structural steel, with a Young's modulus of 200 GPa, Poisson's ratio of 0.30, and yield strength of 250 MPa, was assigned to all tubular members to replicate the mechanical behavior of ASTM A36 mild steel. This material substitution aligns with the validated equivalence of structural steel to mild steel in terms of yield strength and ductility, ensuring that stress results exceeding 250 MPa in simulations indicate yielding in a physical chassis. The tubular members were discretized using BEAM188 elements, a 3D quadratic beam formulation optimized for slender structures. A uniform mesh size of 133 mm was applied across all designs, ensuring at least two elements per shortest member (e.g., cross-members, vertical braces) and sufficient resolution along longer components (e.g., side rails, main hoops). Mesh independence was confirmed through a convergence study, where further refinement to 100 mm resulted in less than 5% variation in peak stress values. Welded joints were modelled as rigid connections to reflect typical spaceframe fabrication practices. The details on the number of elements and nodes on each design mesh are in Table 1.

TABLE 1: Meshing parameters

Design	Elements	Nodes	Element Type	Mesh Size
Design 1	541,878	884,144	BEAM188	133 mm
Design 2	552,397	891,218	BEAM188	133 mm
Design 3	571,413	903,876	BEAM188	133 mm

Fixed boundary conditions were applied at critical nodes to simulate real-world constraints: front bulkhead nodes for crash structure mounting, main roll hoop base nodes for rollover grounding, front hoop base nodes for braking load transfer, suspension mounts (wheel hubs, engine brackets) for subsystem anchoring, and rear bulkhead nodes for torsional isolation. All degrees of freedom (translational and rotational) were restricted at these points to replicate vehicle-chassis interactions (Figures 4a - 4e). Linear elastic analysis was conducted to evaluate stress distributions, with regions exceeding the 250 MPa yield threshold flagged as critical failure zones. The BEAM188 element was selected for its computational efficiency and accuracy in modelling slender tubular geometries and welded joints, ensuring reliable predictions of stress and deformation under static loads.

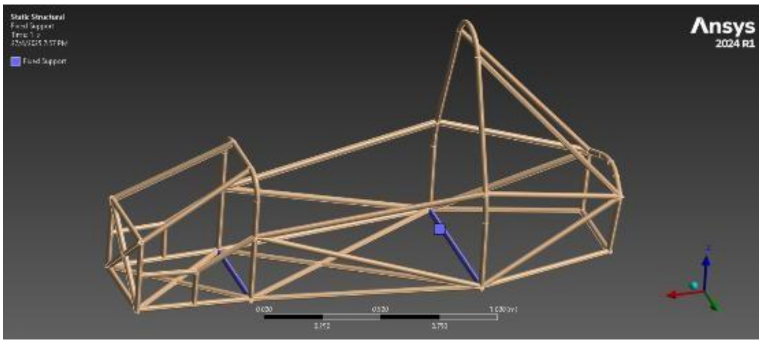

(a)

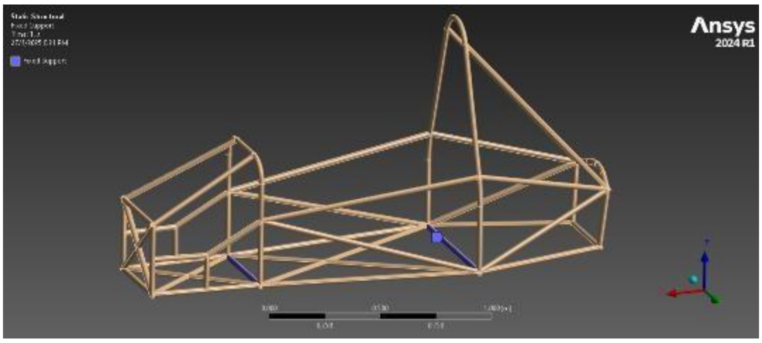

(b)

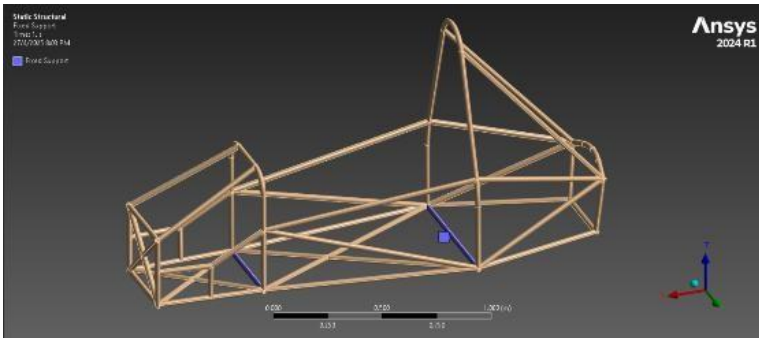

(c)

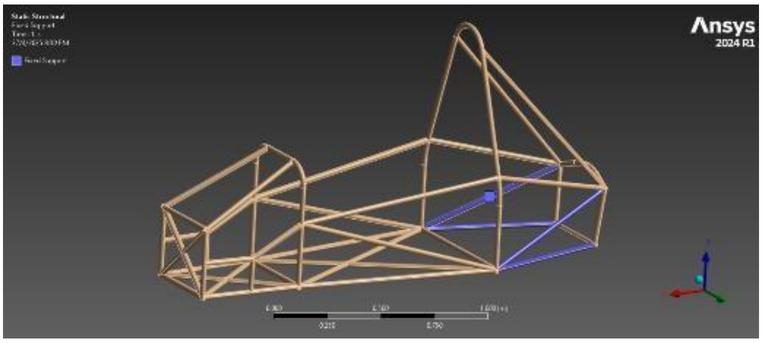

(d)

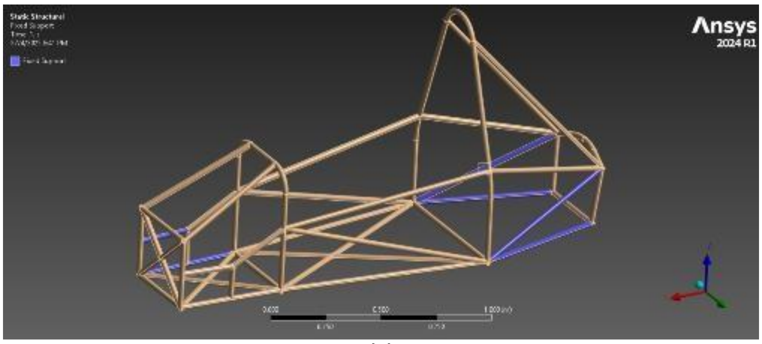

(e)

FIGURE 4: Fixed support setting at (a) front bulkhead nodes, (b) main roll hoop base, (c) front hoop base, (d) suspension mounts, (e) rear bulkhead

2.3 Static Load Cases

Five static load cases were simulated to evaluate the chassis' structural integrity under extreme operational and crash scenarios. Each case applied a concentrated 10 kN force to replicate severe loading conditions, covering critical directions mandated by FSAE standards. These scenarios included frontal impacts, rollover forces, braking loads, lateral impacts, and torsional deformation, as shown in Table 2.

TABLE 2: Static load case summary

Load Case	Force Application	Constraints	Objective
Front Impact	10 kN horizontal at front bulkhead	Rear bulkhead fixed	Test frontal crashworthiness
Main Roll Hoop Load	10 kN lateral at roll hoop apex	Base of main hoop fixed	Validate rollover protection
Front Hoop Load	10 kN rearward at front hoop apex	Front hoop base fixed	Assess braking load transfer
Lateral Shear	10 kN transverse at mid- side nodes	Opposite side fixed	Evaluate side intrusion resistance
Torsional Loading	10 kN vertical (up/down) at front corners	Rear bulkhead fixed	Measure torsional rigidity

For each load case, stress distributions and deformations were analyzed to identify critical regions. The front impact test simulated a 70 km/h collision by constraining the rear bulkhead and applying force at the front nodes. The main roll hoop load exceeded FSAE's 1.5 times vehicle weight requirement to ensure safety margins. Lateral shear and torsional loading tested the chassis' resistance to side impacts and twisting, respectively. Contour plots with a unified color scale (red: ≥250 MPa, blue: low stress) visualized stress concentrations, while total displacements at key nodes quantified stiffness. Designs were evaluated against a 250 MPa yield threshold, with regions exceeding this limit flagged as failure-prone.

3. RESULTS AND DISCUSSION

3.1 Overview of FEA Outcomes

The peak von Mises stress and total deformation for each chassis design under the respective load cases are summarized in Tables 3 and 4. These simulations were conducted in ANSYS using structural steel material properties, and the results are benchmarked against a mild steel yield criterion of 305 MPa, per FSAE Rule F.3.4.2. Deformation is reported in meters, and stress is presented in Pascals.

TABLE 3: Peak von Mises Stress (Pa)

Load Case	Design 1	Design 2	Design 3
Front Impact (10 kN)	6.49e7	1.7465e8	6.8568e7
Main Roll Hoop Load (10 kN)	6.0118e7	8.3624e7	9.4504e7
Front Hoop Load (10 kN)	3.1272e8	3.2921e8	2.386e8
Lateral Shear (10 kN)	2.7132e8	1.3906e9	4.9407e8
Torsional Loading (10 kN×2)	6.7009e7	1.1728e8	1.5955e8

TABLE 4: Maximum deformation (m)

Load Case	Design 1	Design 2	Design 3
Front Impact (10 kN)	0.000169	0.00075516	0.00055478
Main Roll Hoop Load (10 kN)	0.000634	0.003879	0.00077073
Front Hoop Load (10 kN)	0.0023442	0.0055485	0.0025826
Lateral Shear (10 kN)	0.0031869	0.013229	0.010399
Torsional Loading (10 kN×2)	0.00044877	0.00064379	0.000067396

3.2 Stress Concentration and Load Transfer Analysis

In all loading scenarios, von Mises stress contours reveal critical insights into structural load paths and stress concentration zones. For lateral shear loading, Design 2 experienced the most severe over-stressing at 1.3906×10^9 Pa, significantly surpassing the allowable yield limit. This is illustrated in Figure 5, which shows the von Mises stress distribution under side-impact loading. The overstressed region corresponds to the side bay area with insufficient triangulation, validating the theory that rectangular unbraced regions are susceptible to localized failure.

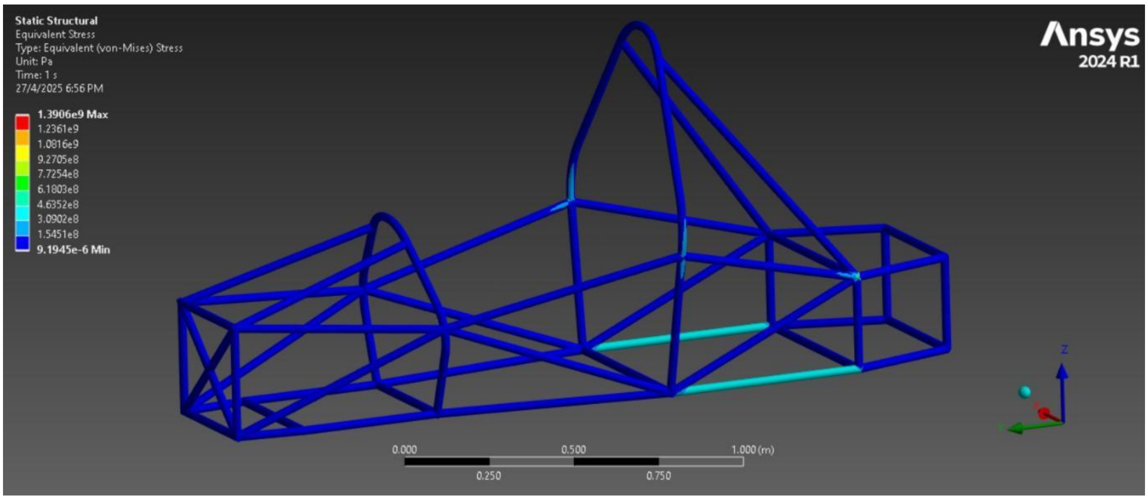

FIGURE 5: Von Mises Stress – Design 2 under side impact

In contrast, Figure 6 displays the stress contours for Design 1 under front impact, showing well-distributed loading across the front hoop and longitudinal members. The stress peaks at approximately 6.49×10^7 Pa, indicating an effective load path and sufficient reinforcement in the frontal zone. Design 3, shown in Figure 7 under front hoop loading, demonstrates superior load distribution due to additional braces connecting the hoop to the side rails and floor members, resulting in lower peak stress of 2.3860×10^8 Pa.

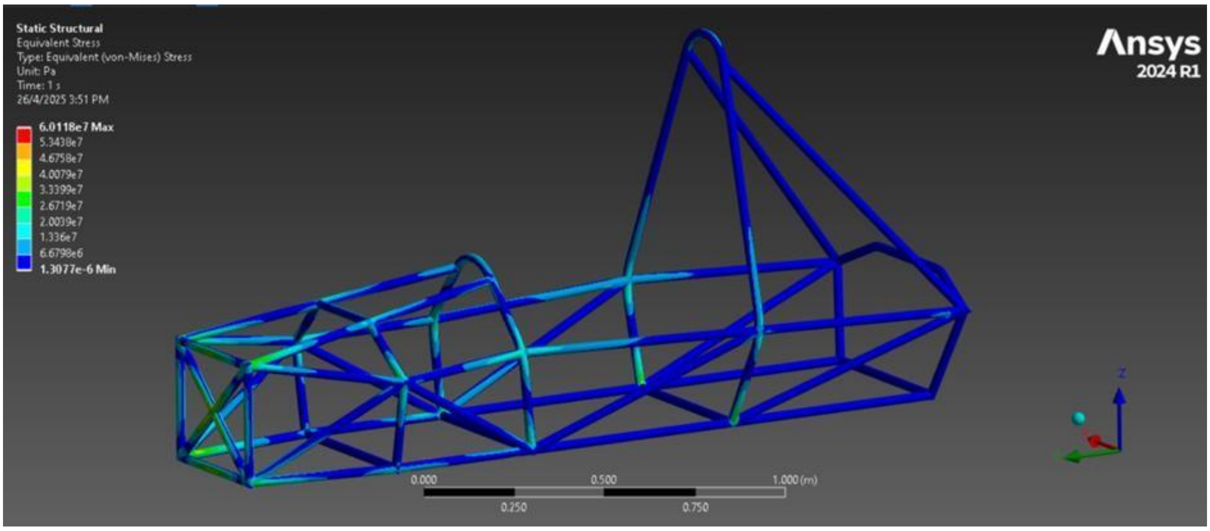

FIGURE 6: Von Mises Stress – Design 1 under Front Impact

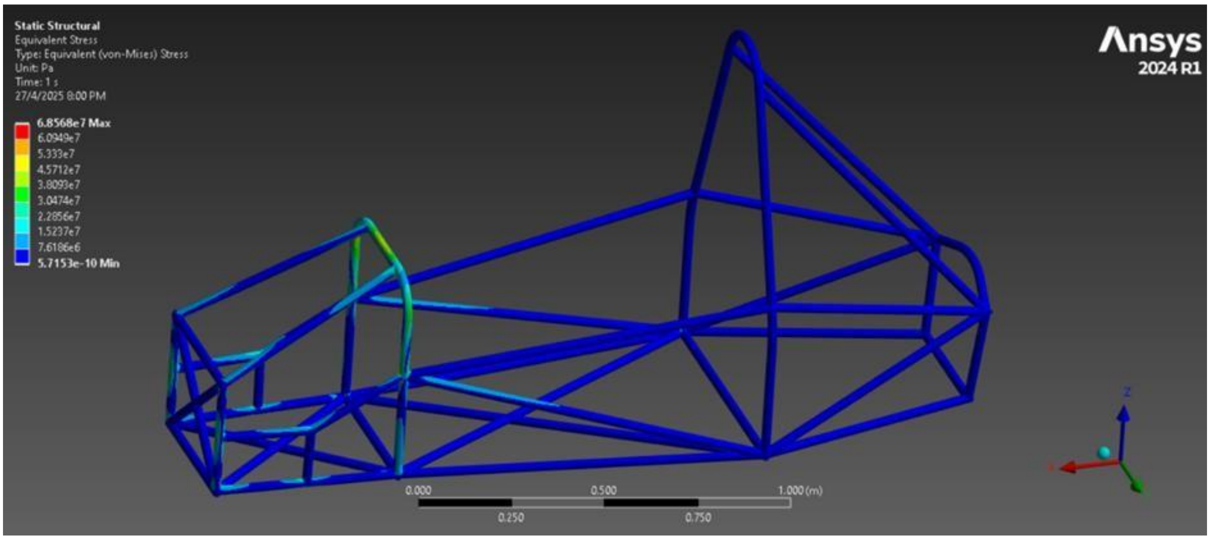

FIGURE 7: Von Mises Stress – Design 3 under Front Hoop Load

Design 3's performance under torsional loading is further substantiated in Figure 8, where the stress remains well distributed within the triangulated substructure and does not exceed critical thresholds, even though it shows higher von Mises values than Design 1. Design 2's torsional stress results (Figure 9) reveal stress localization near the rear bulkhead, indicating poor torque transfer efficiency and potential failure zones during dynamic cornering.

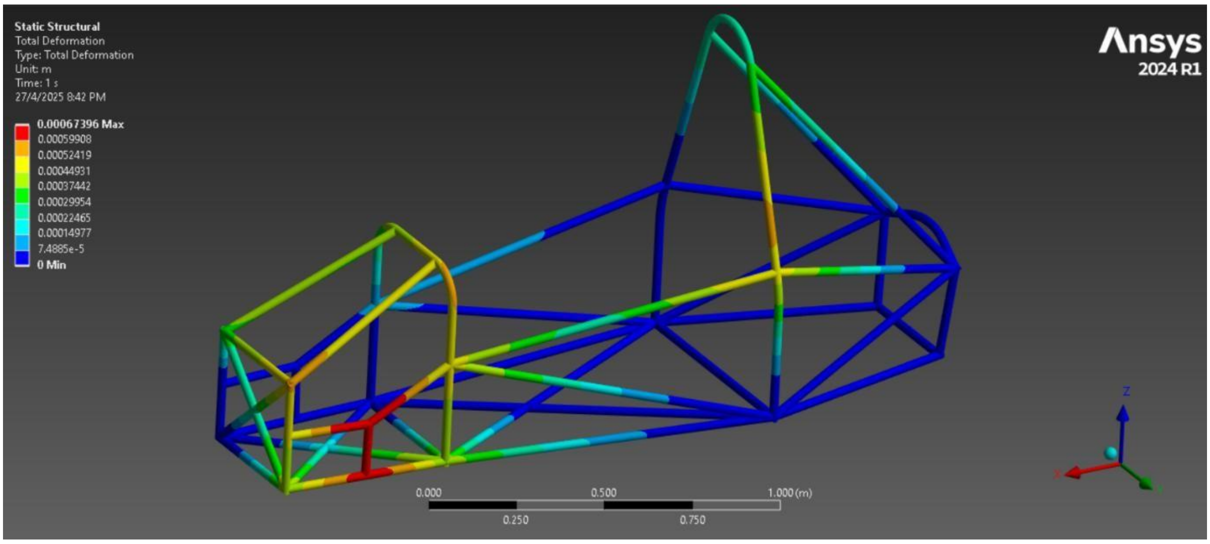

FIGURE 8: Total deformation – Design 3 under Torsional Loading

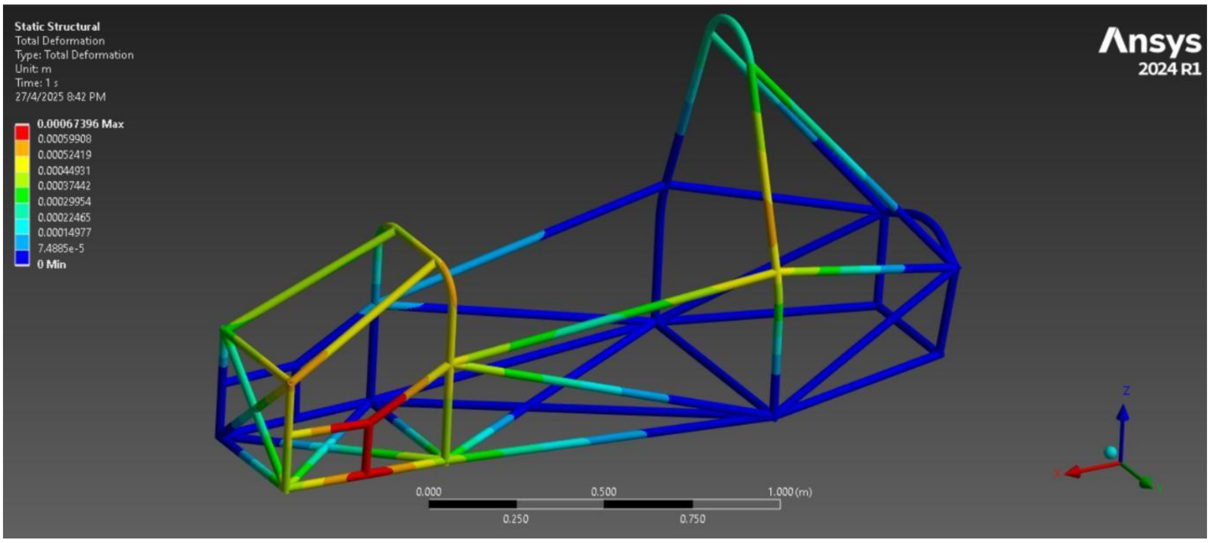

FIGURE 9: Von Mises Stress – Design 2 under Torsional Loading

3.3 Deformation and Structural Rigidity Evaluation

Deformation metrics provide insight into chassis stiffness, a key factor influencing suspension consistency and driver feedback. Figure 10 highlights the excessive deformation in Design 2 under side impact, measuring 13.229 mm. The side structure's lack of X-bracing or diagonal reinforcement allows substantial lateral deflection, compromising driver safety. By comparison, Designs 1 and 3 limit deflection to 3.187 mm and 10.399 mm, respectively. Though Design 3 has higher deformation than Design 1 in this scenario, its stress levels remain better managed, suggesting ductile redistribution without exceeding yield limits.

In the torsional test, Design 3 shows excellent stiffness, with only 0.067 mm of deformation (Figure 8), indicating effective integration of the triangulated floor members. Conversely, Design 1 (Figure 11) deforms by 0.449 mm under the same load, confirming a more flexible chassis prone to twisting. This disparity affects suspension alignment and roll-center stability during high-speed maneuvers.

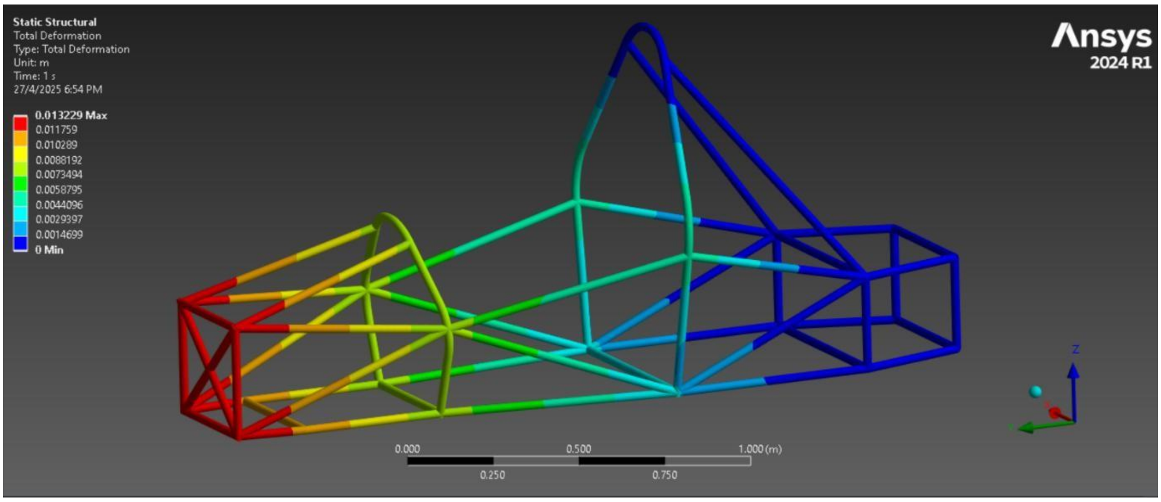

FIGURE 10: Total deformation – Design 2 under side impact

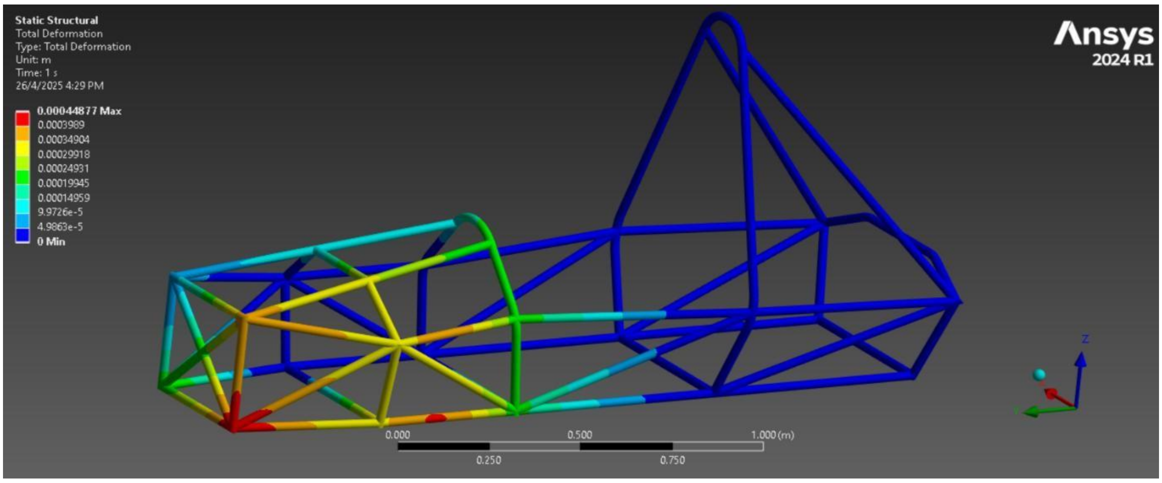

FIGURE 11: Total deformation – Design 1 under torsional loading

3.4 Compliance with Formula SAE Structural Standards

According to FSAE 2025 Rule F.3.4.2, chassis structures must maintain elastic behavior under standardized load tests with baseline steel yield strength set at 305 MPa. Design 1 complies with this standard across all loading scenarios, albeit marginally exceeding 300 MPa under front hoop loading. Design 2 violates this rule under front-hoop and side-impact conditions, both in stress and deformation – showing excessive deflection and high-stress regions beyond permissible limits.

Design 3 performs best overall, breaching the 305 MPa threshold only in side impact stress (494 MPa). While this still necessitates structural refinement, such as adding an X-brace in the cockpit opening, it remains superior in global stiffness and overall compliance. Stress values are generally within acceptable ranges for dynamic performance and safety.

3.5 Load Path Efficiency and Structural Optimization

The comparative analysis underlines the impact of triangulation and node connectivity on load distribution. Design 1 relies on traditional horizontal-vertical framing, resulting in acceptable performance but limited dynamic stiffness. Design 2 compromises these load paths, focusing excessively on weight reduction at the cost of side and hoop reinforcement. Design 3 integrates cross-members and triangulated bays, creating multiple efficient load paths to absorb and redirect forces, as evidenced by the torsional and frontal performance metrics.

This design principle aligns with findings by Barbosa et al. (2024), which showed that the strategic addition of floor and side triangulation improved chassis stiffness by over 50% with a weight increase of less than 5%. Figures 7 and 8 exemplify this in our study, showing that Design 3's superior stress dispersion and reduced structural deformation.

4. CONCLUSION

The comparative Finite Element Analysis (FEA) conducted in this study highlights the critical structural implications of different chassis design philosophies for Formula SAE vehicles. Among the three evaluated configurations, Design 3 demonstrates the most robust and well-rounded performance profile. Its fully triangulated architecture significantly improves torsional stiffness and distributes loads efficiently, resulting in superior stress control and minimal deformation under extreme static loading conditions.

Design 1, while meeting safety standards in most scenarios, exhibits reduced stiffness and marginal compliance under front hoop loads. Conversely, Design 2, which prioritizes weight reduction, fails to meet essential regulatory requirements, particularly under lateral shear and front-hoop scenarios. The high deformation and stress concentrations observed in Design 2 compromise both structural integrity and driver safety.

Design 3 exceeds the 305 MPa yield threshold during side-impact loading; however, its performance remains within a tolerable range and can be rectified with minor structural reinforcements, such as additional bracing in the side-impact region. These adjustments would ensure full compliance with FSAE regulations while maintaining the dynamic benefits of a rigid, triangulated frame.

This study reaffirms the importance of triangulated load paths and efficient node connectivity in optimizing chassis strength and stiffness. By validating these conclusions through high-fidelity simulation and regulatory benchmarking, the findings serve as a valuable reference for future FSAE chassis design iterations aiming to balance safety, performance, and manufacturability.

ACKNOWLEDGEMENT

This research is funded by Perodua's grant and further supported by the organizers of the 2025 Next Generation Vehicle Challenge, which consists of the Malaysian Automotive Robotics & IoT Institute (MARii) and the Society of Automotive Engineers Malaysia (SAEM).

REFERENCES

Alirezaei, M., Noori, M., Tatari, O., Mackie, K. R., & Elgamal, A. (2016). BIM-based damage estimation of buildings under earthquake loading conditions. Procedia Engineering, 145, 1051-1058.

Barbosa, L. M. Q., Fernandes, G. H. N., & de Queiroz Murad, M. (2024). Finite element analysis and optimization of a Formula SAE car chassis. Caderno Pedagógico, 21(1), 2053-2071.

Chen, M. T., & Harichandran, R. (1998). Statistics of the von Mises stress response for structures subjected to random excitations. Shock and Vibration, 5(1), 13-21.

Khot, M., Chinmya, K. A., Mahesh, S., Suprith, S., & Manish, M. (2025). Selection of Materials, Design and Analysis of FSAE Chassis for Different Engineering Application- A Comprehensive Review. International Journal of Automotive Science And Technology, 9(1), 136-157.

Khutal, K., Kathiresan, G., Ashok, K., Simhachalam, B., & Jebaseelan, D. D. (2020). Design validation methodology for bicycle frames using finite element analysis. Materials Today: Proceedings, 22, 1861-1869.

Lim, J. W., & Sivaguru, S. (2018). Chassis structural design of track racing one manned formula car. International Journal of Engineering and Technology, 7(3), 71-75.

Patel, R., Lu, M., Diermann, S. H., Wu, A., Pettit, A., & Huang, H. (2019). Deformation behavior of porous PHBV scaffold in compression: A finite element analysis study. Journal of the Mechanical Behavior of Biomedical Materials, 96, 1-8.

Patil, R., & Chikkali, V. (2020). FEA analysis of FSAE chassis. Carbon, 100, 0-280.

Riley, W. B., & George, A. R. (2002). Design, analysis and testing of a formula sae car chassis (No. 2002-01-3300). SAE Technical Paper.

SAE (2024). Formula SAE Rules 2025. SAE International.

Stava, O., Vanek, J., Benes, B., Carr, N., & Měch, R. (2012). Stress relief: Improving structural strength of 3D printable objects. ACM Transactions on Graphics (TOG), 31(4), 1-11.

Thosar, S., Mutha, A., & Dharurkar, S. A. (2016). Structural performance analysis of SAE Supra Chassis. In Innovative Design and Development Practices in Aerospace and Automotive Engineering: I-DAD, February 22-24, 2016 (pp. 239-252). Singapore: Springer Nature Singapore.

Ulizio, M., Lampman, D., Rustagi, M., Skeen, J., & Walawender, C. (2017). Practical design considerations for lightweight windshield applications. SAE International Journal of Transportation Safety, 5(1), 47-57.

Vijayan, S. N., & Sendhilkumar, S. (2015). Structural analysis of automotive chassis considering cross-section and material. International Journal of Mechanical Engineering and Automation, 2(8), 370-376.

Wang, Y. H., Zhang, C., Su, Y. Q., Shang, L. Y., & Zhang, T. (2020). Structure optimization of the frame based on response surface method. International Journal of Structural Integrity, 11(3), 411-425.